Excited state dynamics in clusters of oxygen

**Runjun Li, Karl A. Hanold, Mark C. Garner, A. Khai Luong
and Robert E. Continetti**

*University of California, San Diego, Department of Chemistry and Biochemistry, 9500
Gilman Drive, La Jolla, CA 92093–0314, USA*

Considerable insights into the dynamics of both ionic (photodissociation) and neutral (dissociative photodetachment) decomposition pathways of O_4^- and O_6^- have been gained using photoelectron and photofragment translational spectroscopy in a fast-ion beam. The O_4^- data at 532 nm reveal a novel process involving sequential photodetachment of an electron with a near-zero binding energy from photodissociating O_4^-. Studies of O_6^- at 532 nm reveal that addition of a third O_2 to the O_4^- core leads to a dramatic change in the photodissociation dynamics, producing highly vibrationally excited O_2^- photofragments not observed in the case of O_4^-. At 355 nm, both O_4^- and O_6^- yield vibrationally excited O_2^- photofragments, as observed by autodetachment of the nascent O_2^- ($v \geqslant 5$) $\rightarrow O_2 + e^-$. At 266 nm, photofragment time-of-flight (TOF) measurements on O_6^- and O_4^- show that the dynamics of dissociative photodetachment in O_6^- are only slightly perturbed relative to O_4^-. The anisotropic product angular distribution previously observed in O_4^- is observed to persist in the three-body neutral decomposition $O_6^- + h\nu \rightarrow O_2 + O_2 + O_2 + e^-$. The origins of these diverse phenomena in O_4^- and O_6^- are discussed.

1 Introduction

An understanding of the evolution of chemical dynamics in neutral and anionic clusters as a function of cluster size has been pursued as it may yield essential insights into condensed-phase dynamics.[1,2] Recent advances in this area have included translational energy spectroscopy studies of the photodestruction of cluster ions,[3,4] and more recently time-resolved photodestruction[5] and photoelectron spectroscopy studies[6] of the reaction dynamics of cluster ions. These studies have begun to probe the influence of solvation on the reaction dynamics in small clusters, including the important caging effect well known from the condensed phase in which the solvent prevents separation of the nascent photofragments. We are interested in studying reaction dynamics in both neutral and anionic clusters of oxygen. Oxygen clusters and liquid oxygen have a complicated chemistry due to numerous low-lying electronic states. In this work we combine measurements of photofragment time-of-flight spectra and photoelectron kinetic energy measurements to probe the photodissociation and dissociative photodetachment (DPD) dynamics of small anionic clusters of oxygen. We find that the dynamics of the neutral DPD pathway are affected only slightly by addition of an O_2 to O_4^-, while the branching ratio for the ionic photodissociation pathway is increased, with a dramatic change in dynamics at 532 nm.

The oxygen dimer anion, O_4^-, provides an interesting test case for the study of the influence of cluster size on reaction dynamics. Small anionic clusters of oxygen appear to form around the unusually stable dimer anion of oxygen, O_4^-. In high-pressure mass spectrometry experiments, Hiraoka showed that O_4^- is bound relative to $O_2(^3\Sigma_g^-)$ + O_2^- ($^2\Pi_g$) by 0.46 ± 0.02 eV.[7] Addition of a third O_2 to form O_6^-, however, was

found to release only an additional 0.11 eV, consistent with electrostatic interactions. Posey *et al.* recorded the photoelectron spectrum of O_4^- at 532 nm which was found to be devoid of fine structure with the exception of the characteristic peaks of O_2^- photodetachment.[8] This showed that photodissociation was an important channel at that wavelength, with the nascent O_2^- produced in the primary photodissociation undergoing photodetachment by a second photon:

$$O_4^- + h\nu \rightarrow O_2 + O_2^-(^2\Pi_g)$$

$$O_2^-(^2\Pi_g) + h\nu \rightarrow O_2(^3\Sigma_g^-, {}^1\Delta_g) + e^-$$
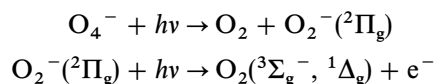
DeLuca *et al.* later studied the photodestruction of O_4^- and higher clusters at 1.06 μm, and observed significant photodissociation of $(O_2)_n^-$, $n \geqslant 3$, in the absence of a strong absorption in O_4^-.[9] They interpreted these results in terms of a charge-transfer-to-solvent absorption in which the excess electron was transferred from the O_4^- core to the 'solvent' O_2. Han and Johnson carried out studies of the nascent O_2^- vibrational distribution ($v = 0$–3) from photodissociation of $(O_2)_n^-$ clusters by photoelectron spectroscopy at 1064 and 532 nm.[10] At 1064 nm, they found a vibrational distribution consistent with a vibrational temperature of 2600 K. Detailed analysis of the 532 nm data was not reported in their paper. There have also been a number of detailed studies on electron attachment to neutral clusters of oxygen by Märk and co-workers, in which the primary event is electron capture by a single O_2 molecule within the cluster environment.[11,12]

In our laboratory we have carried out a further series of experiments designed to clarify the photochemistry of O_4^-. These studies have shown that O_4^- undergoes two limiting photodestruction processes in the wavelength range from 532 to 262 nm: photodissociation $(O_4^- + h\nu \rightarrow O_2^- + O_2)$ and dissociative photodetachment $(O_4^- + h\nu \rightarrow O_2 + O_2 + e^-)$.[13–15] Both processes occur on repulsive excited state potential energy surfaces, leading to large translational energy release and highly anisotropic product angular distributions.

The photodissociation studies[14] confirmed the bond dissociation energy for $O_4^- \rightarrow O_2^- + O_2$ and also demonstrated that the lowest energy photodissociation channel at wavelengths less than 532 nm yields excited $O_2(^1\Delta_g)$ and ground state $O_2^-(^2\Pi_g)$ products. This shows that the ground electronic state of O_4^- is most likely a doublet state since the dissociation of a quartet state into a singlet and doublet is spin-forbidden. The photodissociation dynamics exhibit a marked wavelength dependence. At both 523 and 532 nm, photodissociation yields a very narrow photofragment distribution: 90% $O_2(^1\Delta_g, v = 0) + O_2^-(^2\Pi_g, v = 0)$ and 10% $O_2(^1\Delta_g, v = 0) + O_2^-(^2\Pi_g, v = 1)$, with low rotational excitation. At 349, 355, 262 and 266 nm, however, the photofragments were found to be vibrationally and rotationally excited. In addition, evidence for the production of electronically excited $O_2(^1\Sigma_g^+)$ products was observed at 262 nm. The photodissociation product angular distributions at all wavelengths were found to be strongly peaked along the electric vector, with an anisotropy parameter β[16] ranging from 1.8 to 2.0 as the photon energy increases. These results showed that there are several optically allowed low-lying repulsive states of O_4^- accessed by a parallel transition from the ground state.

The studies of dissociative photodetachment (DPD) have revealed considerable insights into both the structure of O_4^- and the repulsive states of O_4. At 532 nm, we recorded high resolution photoelectron–photofragment energy correlation spectra for the DPD of O_4^-. Measurement of photoelectron and photofragment kinetic energies in coincidence revealed vibrationally resolved total translational energy release spectra for the process $O_4^- + h\nu \rightarrow O_2(^3\Sigma_g^-, v) + O_2(^3\Sigma_g^-, v) + e^-$. Structural information on gas-phase O_4^- was obtained from this measurement of the correlated O_2 product vibrational distribution using a simple Franck–Condon simulation of the overlap of the

vibrational wavefunctions of two perturbed O_2 molecules with two free ground state O_2 molecules. The simulation showed that two equal O—O bond lengths of 1.272 Å in O_4^-, with a longer O_2—O_2 bond distance inferred, was most consistent with the experimental results. The narrow rotational distributions observed in this experiment indicated that the O_4^- structure is probably characterized by a high symmetry.[15] The observation of non-Franck–Condon photodetachment processes at 349 nm[13] and excited state $O_2(^1\Delta_g) + O_2(^3\Sigma_g^-)$ products at 349, 355 and 266 nm[17] has shown that there are also several repulsive states of neutral O_4 optically accessible from the O_4^- ground state.

Recently, an extensive set of high-level *ab initio* calculations on the ground and excited states of O_4^- has been completed by Aquino *et al.*[18] Using the complete-active-space + second-order perturbation theory (CASPT2) method,[19] they have obtained predictions for the structure, electron affinity, bond dissociation energy and vibrational frequencies of O_4^-. The large aug-cc-pVTZ basis,[20] known to give reliable values for electron affinities of first-row atoms and molecules, was used. These calculations predict that the equilibrium structure of O_4^- has D_{2h} symmetry with a ^2A_u electronic ground state. The stability of O_4^- with respect to $O_2(^3\Sigma_g^-) + O_2^-(^2\Pi_g)$ is calculated to be *ca.* 0.50 eV, in reasonable agreement with the experimental quantities.[14] The calculations show that the electronic structure of O_4^- is a notoriously multi-configurational problem; however, the ^2A_u ground state may be rationalized in terms of the dominant configuration by considering overlap of the π_g anti-bonding orbitals of O_2 and O_2^- as shown in Fig. 1.

Aquino *et al.*[18] have also examined the doublet excited states of O_4^-. In particular, they have located three excited states optically accessible from the ^2A_u ground state of O_4^- *via* a parallel transition (polarized along the x-axis in D_{2h} symmetry as shown in Fig. 1). Fig. 2 shows a pseudo-diatomic schematic view of these excited states in terms of
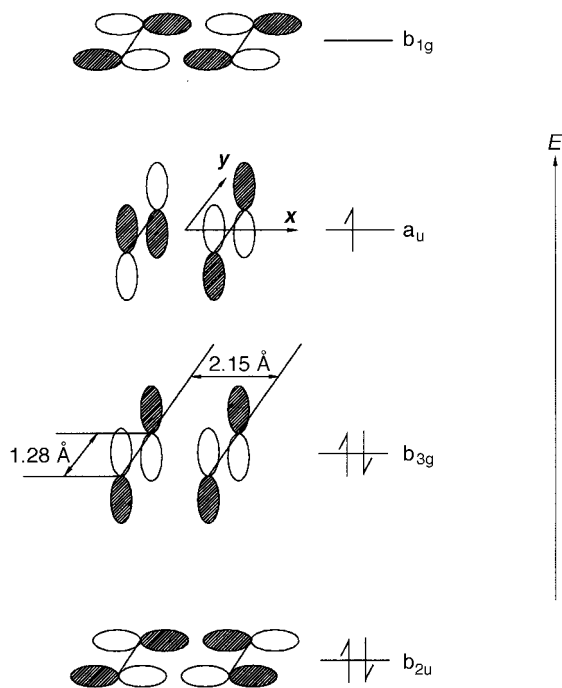
Fig. 1 Qualitative molecular orbital model for the ^2A_u ground state of O_4^-. The D_{2h} symmetry axes and theoretical predictions of the bond lengths are also shown.
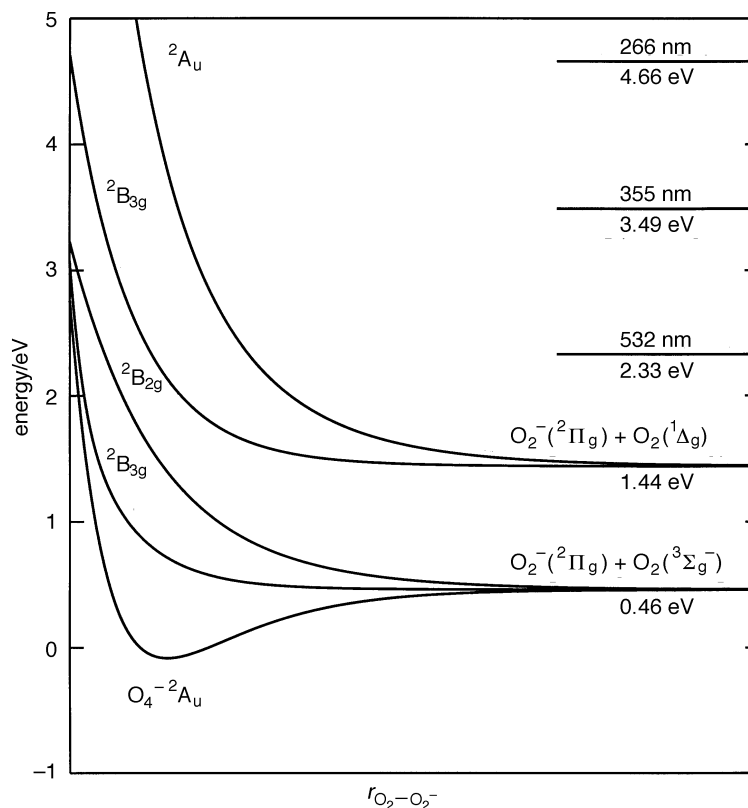
Fig. 2 Schematic ground and dipole-allowed excited-state potential energy surfaces for O_4^-. The adiabatic correlations for the low-lying doublet excited states are shown, with experimental energetics[14] for the dissociation channels. The relative energies of the $^2B_{3g}$ and ^2A_u excited states are from theoretical calculations[18] as described in the text.

the O_2—O_2^- distance. Electric-dipole absorption along the x-axis can occur to repulsive $^2B_{3g}$ excited states, with one at 0.66 eV above the ground state correlating to $O_2(^3\Sigma_g^-) + O_2^-$ ($^2\Pi_g$) products. There is a second repulsive $^2B_{3g}$ excited state correlating to $O_2(^1\Delta_g) + O_2^-$ ($^2\Pi_g$) products at 2.0 eV above the ground state. Excitation to this state may explain the observation at 532 nm of this channel with low vibrational excitation. Finally, at 4.5 eV above the ground state is a ^2A_u repulsive state. This state becomes vibronically allowed with excitation of the b_{3u} vibration of O_4^-. The b_{3u} vibration lengthens one O—O bond while shortening the other one, breaking the D_{2h} symmetry and resulting in localization of the excess electron on the incipient O_2^-. Thus, this state might be expected to be strongly coupled to the photodissociation reaction. The calculated energy of this state is too high to explain the observation of highly vibrationally excited products at 355 nm (3.5 eV). This seems to be a possibility worthy of further consideration, however, as involvement of this state may provide an explanation for the sharply differing photodissociation dynamics in O_4^- at 532 and 355 nm.

In the present work, we aim to experimentally address the influence on the reaction dynamics of the addition of a third O_2 molecule to form O_6^-. We also provide additional information on the photodissociation dynamics of O_4^-. Theoretically, the O_6^- cluster is an open question, as no calculations known to us have been carried out on the structure of this cluster to date. As mentioned above, though, it is known experimentally that the third O_2 is bound much more weakly than the dimer binding energy. The

influence of clustering on these photodestruction pathways will be addressed *via* a combination of photoelectron and photofragment translational spectroscopy. The effect on the photodissociation channel is studied by examination of the photoelectron spectra of O_4^- and O_6^-. Photoelectron spectra can provide information on the photodissociation channel in two ways. As shown by Johnson and co-workers,[8–10] sequential photodetachment of photofragments $O_2^-(v < 3)$ can provide insights into the nascent distribution of $O_2^-(v = 0–3)$. The second way is due to the facile autodetachment of $O_2^-(v > 3)$. Given a photoelectron spectrometer with good low-electron-energy transmission, the characteristic autodetachment peaks of $O_2^-(v)$ can be observed as a tell-tale sign of highly vibrationally excited O_2^-. Initial studies of the photofragment energy and angular distributions produced in the DPD of O_6^- are also presented, as studied by time-of-flight spectroscopy and interpreted *via* Monte Carlo simulations.

2   Experimental

The dissociative photodetachment spectrometer used in these experiments has been previously described in detail,[13,21] and only a brief overview will be given here. Oxygen cluster anions are produced in a pulsed supersonic expansion at a repetition rate of 1 kHz by electron impact on either pure O_2 or 2–5% O_3 seeded in He–Ne with a 1 keV electron beam. Anions are formed by secondary electron attachment processes and cooled by collisions in the expansion. The anions pass through a skimmer to enter a differentially pumped chamber, are accelerated to beam energies of 2.5–4 keV, and mass-selected by time-of-flight. In the interaction region the ion packet is intercepted orthogonally by the linearly polarized 100 ps pulsed output of a mode-locked, Q-switched, cavity-dumped Nd : YAG laser using the harmonics at 532, 355 or 266 nm. The laser was focused to a spot of *ca.* 0.5 mm diameter, yielding fluences of *ca.* 700 MW cm^{-2} at 532 nm and *ca.* 200 MW cm^{-2} at 355 and 266 nm. The laser electric vector, E, was rotated with respected to the beam velocity using a half-wave plate.

The laboratory kinetic energy and recoil angle of photodetached electrons are determined by time-of-flight using a time- and position-sensitive photoelectron detector.[21] The photoelectron recoil angle must be measured to allow correction for the large Doppler effect in the fast ion beam. The center-of-mass electron kinetic energy ($E_{k, e}$) resolution is *ca.* 4% $\Delta E/E$. Calibration using the photodetachment of O_2^- showed peak-position accuracy of <5 meV from $E_{k, e} = 0.2–2$ eV at 532 nm and <10 meV from 1 to 3 eV at 355 nm. The use of a short-pulse laser allows these measurements to be made with an extremely short (7.5 cm) flight path. This facilitates the transmission of low energy electrons ($E_{k, e} < 200$ meV), allowing studies of vibrationally autodetaching O_2^-.

If the ion or neutral dissociates after photon absorption, the photofragments recoil out of the beam over a 0.95 m flight path and impinge on a two-particle time- and position-sensitive detector. In the case of two-body dissociation, photofragments are determined to originate from a single dissociation event by checking for conservation of linear momentum in the center-of-mass frame. In experiments on O_6^-, however, three O_2 products are anticipated, so the primary observable from the photofragments is the time-of-flight (TOF) spectrum on the two halves of the detector. The overall time-of-flight distribution can be measured and simulated, however. Measurements were made of neutral-only photofragment TOF distributions by electrostatically deflecting any residual ions and ionic photofragments out of the beam path after the laser interaction region.

3   Results

532 nm photoelectron spectra: O_4^- and O_6^-

In Fig. 3 photoelectron spectra from O_4^- and O_6^- are shown in the bottom and top frames, respectively. Both photoelectron spectra are dominated by a broad feature
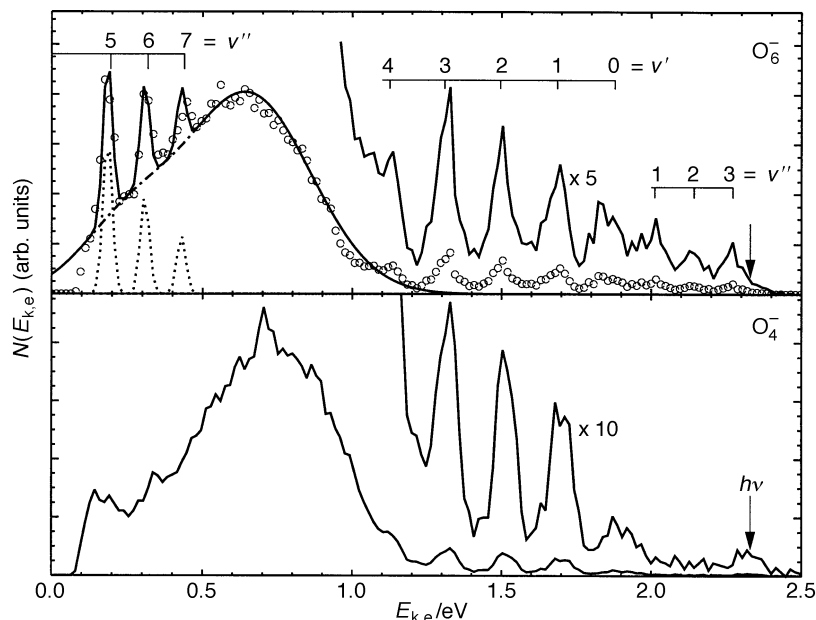
Fig. 3 Top frame: photoelectron spectrum of O_6^- at 532 nm. Autodetachment peaks are labelled $v'' = 5, 6, 7$ and sequential photodetachment peaks from O_2^- shown in the $\times 5$ trace. The peaks labelled $v' = 0, 1, 2, 3, 4$ correspond to photodetachment of $O_2^-(v'' = 0)$ to the labelled state of O_2. The peaks labelled $v'' = 1, 2, 3$ correspond to photodetachment of $O_2^-(v'')$ to $O_2(v' = 0)$. The fit to the broad DPD feature and sharp autodetachment peaks was used to extract an estimate of the relative cross sections for production of $O_2^-(v'' \geqslant 5)$. Bottom frame: photoelectron spectrum of O_4^- at 532 nm. Sequential photodetachment peaks from O_2^- shown in $\times 10$ trace. Note peak at the photon energy ($h\nu$).

peaking at 0.7 (O_4^-) and 0.6 eV (O_6^-). This feature has been shown in our previous studies of O_4^- to be due to DPD on a repulsive neutral surface: $O_4^- + h\nu \rightarrow O_2(^3\Sigma_g^-)$ $+ O_2(^3\Sigma_g^-) + e^-$. It is likely that the origin of this feature is identical for O_6^-, with the third O_2 produced in the electronic ground state. Beyond that, however, the spectra show considerable differences. The fine structure observed in the O_4^- spectrum (see $\times 10$ trace) originates from the primary photodissociation process $O_4^- + h\nu \rightarrow O_2(^1\Delta_g,$ $v = 0) + O_2^-(^2\Pi_g, v = 0,1)$ followed by photodetachment of the O_2^- photofragment with a second photon.[8,13,15] The features in the photoelectron spectrum at 0.15 and 0.35 eV also arise from the photodetachment of nascent O_2^- and an additional small peak reproducibly appears at the photon energy (2.33 eV).

In the case of O_4^-, photoelectron–photofragment coincidence experiments have been carried out.[15] These experiments allow the photoelectron spectrum of nascent O_2^- photofragments at 532 nm to be studied in greater detail by examining only photoelectrons produced in coincidence with photodissociation events characterized by kinetic energy release, E_T, in the range 0.7 to 0.9 eV. This spectrum is shown in the middle frame of Fig. 4, and the photoelectron spectrum of free O_2^- is shown in the bottom frame for reference. The peak positions for the photodissociated O_2^- agree well with the photoelectron spectrum of free O_2^-. There is, however, a dramatic difference between the relative intensities of the $O_2(^3\Sigma_g^-)$ and $O_2(^1\Delta_g)$ manifolds and those of free O_2^-. As discussed below, this is likely to be due to the molecular-frame photoelectron angular distribution for $O_2^- + h\nu \rightarrow O_2 + e^-$ and the fact that the $O_2 + O_2^-$ products of the photodissociation are strongly aligned by a parallel electronic transition with $\beta \approx 1.8$.[13]
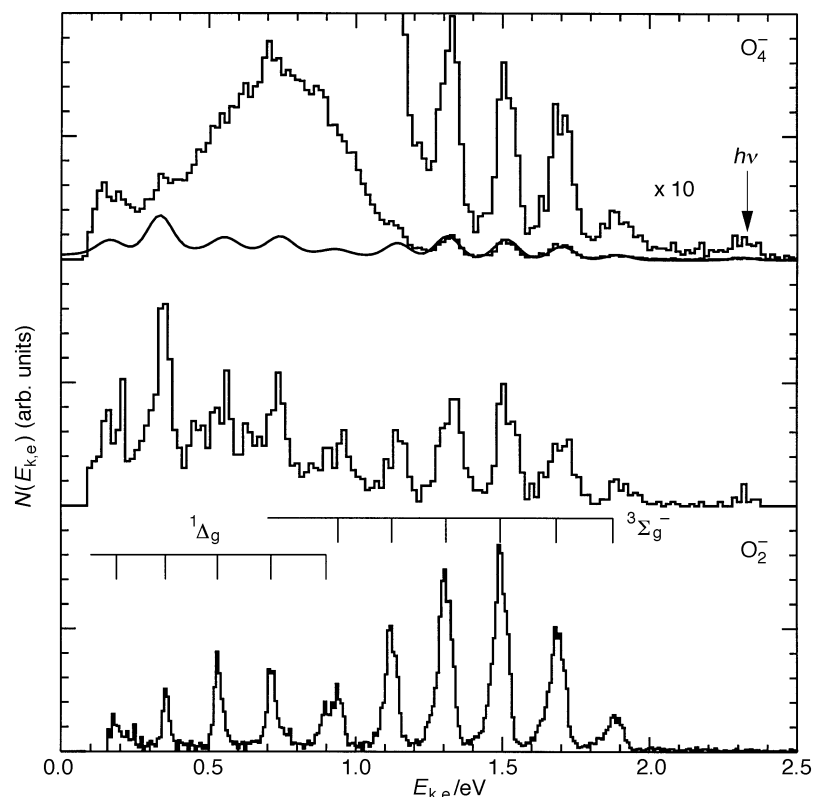
Fig. 4 Top frame: photoelectron spectrum for O_4^- as shown in Fig. 3. Middle frame: energy-gated photoelectron spectra of O_4^- at 532 nm, found by binning only photoelectrons produced in coincidence with photofragment translational energy release $0.7 < E_T < 0.9$ eV. Bottom frame: photoelectron spectrum of free O_2^-, with product O_2 electronic and vibrational states identified with the combs.

The peak at the photon energy is also present in this gated photoelectron spectrum, showing that this is a two photon process: the first photon initiates the photo-dissociation of O_4^-, and the second photon ejects an electron with a near-zero binding energy. This feature was also observed in the earlier work of Han and Johnson[10] and was assigned to photodetachment of $O_2^-(v = 3)$. However, the coincidence measurement of the photofragment translational energy release show that this cannot be true energetically. Possible origins of this novel feature will be discussed further below.

In the O_6^- spectrum in the top frame of Fig. 3 the peak at the photon energy is no longer distinct; however, the region from 2.0 to 2.3 eV is considerably more congested due to the production of vibrationally excited O_2^- in the photodissociation of O_6^-, as previously discussed by Han and Johnson.[10] These features are labelled as $v'' = 1, 2$ and 3 in the $\times 5$ trace on the figure. The most striking difference from the O_4^- spectrum, however, is the appearance of the prominent sharp peaks at 0.19, 0.30 and 0.41 eV labelled as $v'' = 5, 6$ and 7. These peaks can be energetically identified as resulting from the autodetachment of vibrationally excited $O_2^- : O_2(v' = 0) \leftarrow O_2^-(v'' = 5, 6$ and 7).[22,23] The fit to the spectrum allows an estimate of the magnitude of the autodetachment features to be extracted, yielding a vibrational distribution in $v'' = 5 : 6 : 7$ of $0.5 : 0.3 : 0.2$, respectively. The autodetachment peaks have FWHM ≈ 50 meV. These photoelectron spectra confirm that a large change in the photodissociation dynamics producing O_2^- occurs when an O_2 is added to the O_4^- core. The effect on the DPD

process, however, appears to be minimal based on the small change in the photoelectron spectrum.

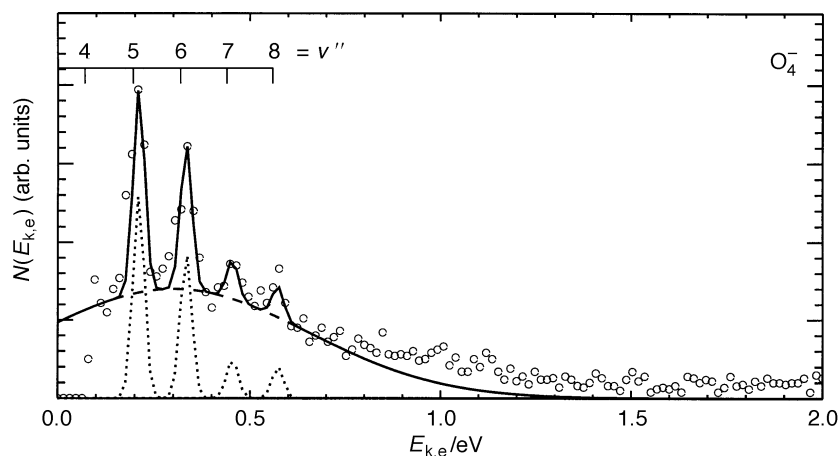## 355 nm photoelectron spectra: O_4^- and O_6^-

The 355 nm photoelectron spectra for O_4^- and O_6^- are shown in Fig. 5. The O_4^- spectrum, in the bottom frame, is dominated by two broad continua, the feature A with a peak at 1.95 eV and a secondary maximum at 1.73 eV and the broad feature B rising below 1.2 eV. The feature A has been previously shown to be due to DPD to ground state $O_2(^3\Sigma_g^-)$ molecules.[13] The two maxima in A arise from the photoelectrons produced in the DPD processes $O_2(v = 0) + O_2(v = 1) + e^-$ and the nearly degenerate $O_2(v = 1) + O_2(v = 1) + e^-$ and $O_2(v = 0) + O_2(v = 2) + e^-$ channels. These features are not observed in the O_4^- photoelectron at 532 nm due to the underlying photodetachment signal of O_2^- as shown in Fig. 4. The broad feature B has been shown to be due to DPD to the new open channel producing $O_2(^3\Sigma_g^-) + O_2(^1\Delta_g) + e^-$.[13] There is additional fine structure superimposed on B at $E_{k,e} < 0.7$ eV. The peak positions are the same $E_{k,e}$ as those observed for O_6^- in the 532 nm data, indicating that these features also correspond to vibrationally autodetaching O_2^- : $O_2(v' = 0) + e^- \leftarrow O_2^-(v'' = 5, 6, 7, 8)$.

This observation of autodetaching O_2^- at 355 nm in the photodissociation of O_4^- is not surprising based on previous photofragment translational spectroscopy measurements in this laboratory.[14] These earlier experiments showed that O_2^- was produced with a wide range of internal excitation. Once again taking advantage of photoelectron–photofragment coincidence measurements on O_4^- at 355 nm, these autodetachment
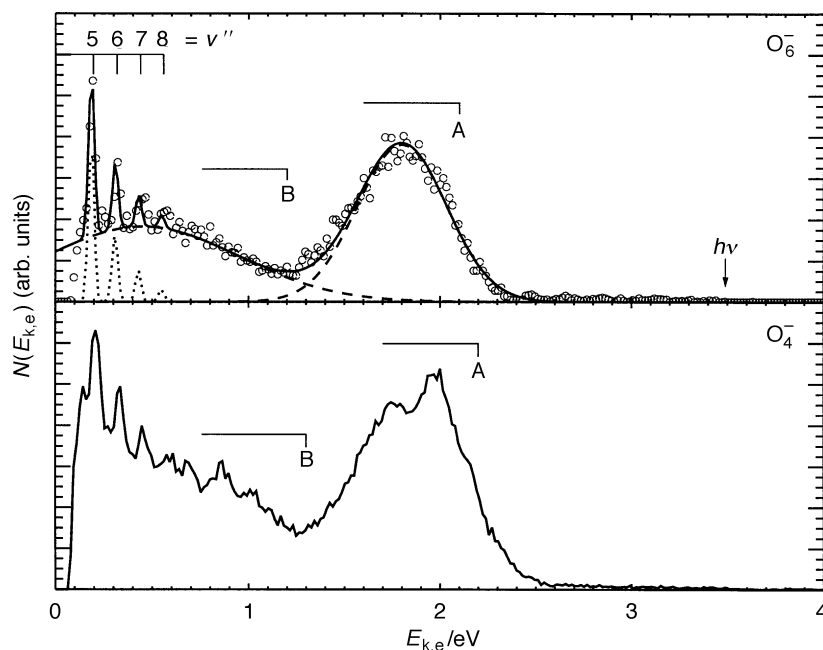
Fig. 5 Top frame: photoelectron spectrum of O_6^- at 355 nm. The autodetachment peaks are labelled $v'' = 5, 6, 7, 8$. The fit to the broad DPD feature and sharp autodetachment peaks was used to extract an estimate of the relative cross-sections for production of $O_2^-(v'' \geqslant 5)$. Bottom frame: photoelectron spectrum of O_4^- at 355 nm. Autodetachment peaks are seen as labelled in top frame.

Fig. 6 Energy-gated photoelectron spectra of O_4^- at 355 nm, found by binning only photoelectrons produced in coincidence with photofragment translational energy release $E_T > 1.1$ eV. The fit to the broad DPD feature and sharp autodetachment peaks was used to extract an estimate of the relative cross-sections for production of $O_2^-(v'' \geqslant 5)$.

features can be examined by generating a spectrum from only those events with $E_T > 1.1$ eV.[17] The spectrum in Fig. 6 shows the autodetachment peaks from O_4^- more clearly due to discrimination against the 'direct' DPD electrons produced in coincidence with lower E_T events. The fit to the spectrum provides an estimate for the intensity of the O_2^- ($v'' = 5, 6, 7, 8$) vibrational state of $0.48 : 0.35 : 0.09 : 0.08$, respectively. The autodetachment peak widths are similar to those observed in the O_6^- spectrum at 532 nm.

The O_6^- photoelectron spectrum is shown in the top frame of Fig. 5. The broad continua, A and B, are very similar to the O_4^- spectrum, suggesting that DPD to both $O_2(^3\Sigma_g^-) + O_2(^3\Sigma_g^-) + e^-$ and $O_2(^3\Sigma_g^-) + O_2(^1\Delta_g) + e^-$ occurs in O_6^- as well. The third, weakly bound O_2 is presumably produced in the electronic ground state. The features are shifted to lower electron kinetic energies (higher electron binding energies) than in O_4^- by approximately 100 meV. The striking feature in the spectrum, however, is the prominence of the autodetachment peaks in O_6^-. This suggests that the photodissociation cross-section is significantly higher in O_6^- than in O_4^- at this wavelength. The vibrational distribution does not appear to show a great difference between the two species, however. The fit to the autodetachment peaks in the spectrum indicates a $v = 5 : 6 : 7 : 8$ distribution of $0.59 : 0.25 : 0.11 : 0.05$. Compared to the results on O_4^-, it appears that the third O_2 reduces the vibrational excitation of O_2^- photoproducts at 355 nm.

266 nm photoelectron spectra

The 266 nm photoelectron spectra for O_4^- and O_6^- are shown in Fig. 7. The energy resolution is degraded at this wavelength due to the large photoelectron kinetic energy and no significant differences are observed between the two species. Feature B, shown to originate from $O_2(^3\Sigma_g^-) + O_2(^1\Delta_g) + e^-$ in O_4^-,[17] is larger than feature A, a change from the ratio observed at 355 nm. Recent experiments have shown that this is due to the higher photon energy accessing new repulsive states of O_4 correlating with these excited molecular products in DPD.[17] Previous studies of the photodissociation of O_4^- have shown that the photodissociation cross-section is reduced to only *ca.* 10% of the DPD channel at 266 nm. Given this low cross-section and the rising laser-correlated
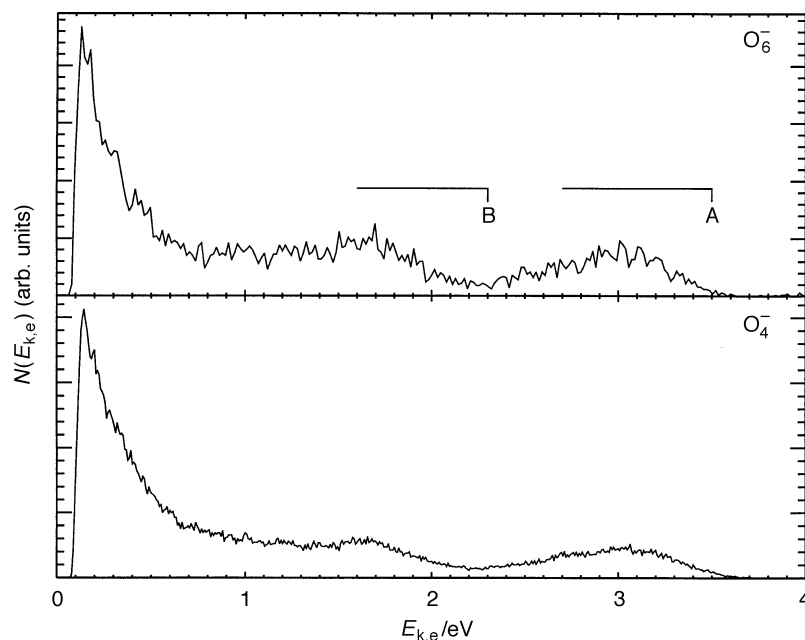
Fig. 7 Top frame: photoelectron spectrum of O_6^- at 266 nm. Bottom frame: photoelectron spectrum of O_4^- at 266 nm. The rising signal below 0.5 eV is due to laser-correlated photoelectrons.

photoelectron background at $E_{k,e} < 0.5$ eV, it is not surprising that autodetachment or sequential photodetachment features are not observable in the spectra.

266 nm neutral photofragment TOF spectra

The dynamics of DPD in O_6^- at 266 nm have been examined by recording photofragment TOF spectra. The translational energy and angular distributions for O_4^- have previously been reported, and show that DPD occurs *via* a parallel transition at all photofragment kinetic energies. At 266 nm the photofragment translational energy release in the DPD of O_4^- peaks at 0.8 eV and has appreciable intensity out to 1.5 eV. The angular distribution is characterized by an anisotropy parameter β that rises from 0.8 to approach the asymptotic value of 2.0 at the higher kinetic energies where significant photodissociation is known to occur.[14] Given the anisotropic product angular distribution, coupled with a large kinetic energy release, photofragment TOF spectra for O_4^- recorded with the $\boldsymbol{E}$ vector of the laser along the ion beam exhibit a winged Doppler profile. The photofragment TOF spectra for O_6^- show the same characteristic shape, as shown in Fig. 8. This figure shows the TOF distribution for the neutral photofragments from O_6^- recorded at a beam energy of 4.0 keV. The TOF is plotted relative to the nominal arrival time of the O_6^- beam at 10.8 μs. The primary difference between the O_6^- TOF spectrum and the O_4^- spectrum (not shown) is the observation of the small peak at the beam velocity of O_6^-. This feature must be due to the 'third' O_2, which, given the similarity in energy and angular distributions to O_4^-, is evidently a spectator which plays little role in momentum conservation in the primary dissociation of the O_4^- core.

To further quantify the similarity between the O_4^- and O_6^- TOF spectra, Monte Carlo simulations were carried out.[14] In these calculations, it was assumed that a two-
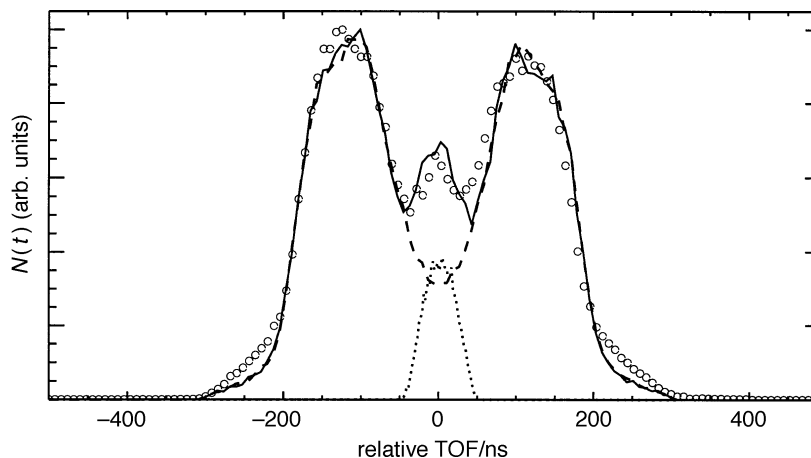
Fig. 8 TOF spectrum of neutral photofragments and $O_6{}^-$ recorded at 266 nm with a beam energy of 4 keV. The nominal arrival time of the center-of-mass is 10.8 μs. The laser E vector was horizontal (along beam axis). The dashed-line fit shows the simulation of the high-energy-release '$O_4{}^-$' channel, and the dotted line fit shows the low-energy-release channel from interaction with the spectator O_2.

body DPD of $O_4{}^- \rightarrow O_2 + O_2 + e^-$ is followed by a two-body interaction between one of the fast O_2 photofragment and the third, spectator, O_2. The DPD of $O_4{}^-$ was modelled using the photofragment energy and angular distributions reported for this process at 262 nm in ref. 14. In the subsequent collision between one of the fast O_2 photofragments and the spectator O_2, the translational energy release is taken to be <0.1 eV and peak at 0 eV in the simulation. As the solid line simulation shows, the agreement between the $O_4{}^-$ DPD center-of-mass energy and angular distributions and the $O_6{}^-$ result is striking. No adjustable parameters were used in this fit other than the fraction of the spectator O_2 detected. Most of the spectator O_2 is not detected in this configuration due to the beam-block at the center of the detector. These results show that the DPD of $O_6{}^-$ is described very well as a two-body dissociation of the $O_4{}^-$ core, with a negligible perturbation by the third O_2. The most noticeable difference between the solid line simulation and the data is the larger signal observed at ± 200 to ± 300 ns. This is signal produced from the high energy part of the photofragment translational energy release distribution, which contains contributions from ion photodissociation.[14] This may indicate an increase in the photodissociation branching ratio at 266 nm as well.

4   Discussion

The photoelectron and photofragment results presented here reveal contrasting effects of the clustering of O_2 with $O_4{}^-$ on the photodestruction dynamics of the $O_4{}^-$ core. $O_4{}^-$ itself is a very interesting species which undergoes photodissociation and DPD at the wavelengths studied in this work. The evidence presented here indicates that addition of a third O_2 increases the relative photodissociation cross-section at 532 and 355 nm. More importantly, the third O_2 causes a drastic change in the photodissociation dynamics at 532 nm, yielding substantial vibrational excitation in the $O_2{}^-$ product, as shown by the autodetaching $v = 5$, 6 and 7 states of $O_2{}^-$ observed at low $E_{k,e}$ in the photoelectron spectra. The continua in the photoelectron spectra associated with DPD, on the other hand, show little change upon clustering with an additional O_2. Furthermore, the TOF spectra recorded for DPD at 266 nm reveal that the translational energy

and angular distribution for the DPD of O_6^- are virtually unchanged from O_4. The third O_2 is truly a spectator with respect to photoexcitation leading to DPD.

## Autodetachment dynamics of O_2^-

The observation of autodetaching states of nascent O_2^- is analogous to the recent observation of vibrationally autodetaching O_2^- formed in dissociative electron attachment to O_3 reported by Allan *et al.*[24] As noted by Allan *et al.*, autodetachment provides a novel probe of the product state distribution in an ionic dissociation yielding an autodetaching molecular anion. The autodetachment peaks observed in the photoelectron spectra for O_6^- at 532 and 355 nm and O_4^- at 355 nm are dominated by maximum Δv autodetachment transitions, *i.e.* $O_2(v' = 0) + e^- \leftarrow O_2^-(v'' = 5)$. In fact, no identifiable peaks associated with other transitions were observed, although given that this signal is on top of a large DPD background, it is unlikely that small peaks associated with other transitions would be easily observable. Autodetachment is known to produce inherently non-Franck–Condon vibrational distributions as it results from a breakdown in the Born–Oppenheimer approximation. As discussed by Schulz, autodetachment in a system like O_2^-, which involves a d-wave ($l = 2$) continuum electron, often favors maximum kinetic energy photoelectrons, as the higher energy electron more readily tunnels through the $l = 2$ centrifugal barrier.[25] The autodetachment features provide a novel probe of O_2^- product vibrational distributions since $O_2^-(v \geqslant 4)$ autodetaches with a quantum yield of unity. Observation of photodetachment by a second photon, $O_2^-(v \leqslant 3) + hv \rightarrow O_2 + e^-$, shown in the 532 nm data, certainly provides a measure of the relative population of those low-lying vibrational states, however, the intensity of this signal is dependent on the square of the laser fluence. Further studies of the product O_2 vibrational distribution in the autodetachment of $O_2^-(v > 3)$ will be of value in extraction of detailed vibrational distributions from the data presented here.

Photodissociation of O_4^-

These experiments provide interesting new insights into the photodissociation dynamics of O_4^-. At 355 nm, the observation of vibrational autodetachment of $O_2^-(v > 5)$ confirms the previous photofragment translational spectroscopy results which indicated the production of O_2^- with significant internal excitation at that wavelength. The peak widths for all of the autodetachment features are observed to be of the order of 50 meV. In the absence of rotational broadening or other perturbations, observation of a 20 meV splitting arising from the spin–orbit states of O_2^- could be expected.[26] Further efforts to determine the rotational distribution of the O_2^- will require a consideration of the propensity rules for vibrotational transitions in autodetachment.[27]

The energy-gated photoelectron spectra recorded at 532 nm reveal two novel results. The first concerns the change in intensity for the $O_2(^3\Sigma_g^-)$ and $O_2(^1\Delta_g)$ channels relative to free O_2. The origin of this effect is most likely due to the fact that the nascent O_2^- produced in the photodissociation of O_4^- is strongly aligned. It is well known that photoelectrons produced in coincidence with the formation of $O_2(^3\Sigma_g^-)$ are characterized by a highly anisotropic laboratory angular distribution peaked perpendicular to the electric vector of the laser, while those corresponding to $O_2(^1\Delta_g)$ are nearly isotropic.[28] The lowest partial wave allowed in photodetachment is a p-wave ($l = 1$).[29] This and the higher partial waves will interfere above threshold and will in general lead to an anisotropic molecular frame photoelectron angular distribution as well.[30] Given the restricted detection geometry in the current experiments, in which photoelectrons are only detected when they recoil into a 20° cone above the ion–laser interaction region, detection of the nearly isotropic photoelectrons produced in coincidence with $O_2(^1\Delta_g)$ is favored.

The more novel result, however, is the observation of a small photoelectron peak at the photon energy. The appearance of this feature at a photofragment translational energy release of 0.8 eV shows unambiguously that the photodetachment process which gives rise to this feature occurs on the repulsive ionic surface correlating to $O_2(^1\Delta_g)$ + $O_2^-(^2\Pi_g)$ after the photofragment repulsion has been determined. In Rydberg states of neutral atoms and molecules and dipole-bound states of negative ions[31,32] it is common to see photoelectrons at nearly the photon energy; however, this is not expected in the case of O_4^-. At the risk of some speculation, consider the following scenario. The excess electron in O_4^- is delocalized over the two O_2 moieties, as shown by experimental[17] and theoretical results.[18] As the O_2 moieties begin to separate in the photodissociation event a point is reached beyond which the electron is localized on one of the O_2. Just before localization occurs, some part of the electronic wavefunction may be in a region of near-zero electron binding energy by analogy to the asymptotic limit of electron transfer between O_2 and O_2^- at large distances, which requires the electron to enter the continuum. If a second photon intercepts the dissociating complex in this configuration, the photoelectron could be ejected with the full photon energy in a two-electron transition:

$$O_4^- + h\nu \rightarrow [O_4^-]^* + h\nu$$

$$\rightarrow O_2(^3\Sigma_g^-, v) + O_2(^3\Sigma_g^-, v) + e^-(E_{k,e} = h\nu).$$
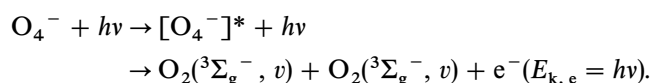
The timescale over which this sequential photon absorption would have to occur is by necessity on a timescale of tens of femtoseconds. The O_2—O_2 distance in O_4^- is calculated to be 2.15 Å. At a kinetic energy of 0.8 eV, this distance will increase by 1 Å in *ca.* 30 fs. For this feature to be observed with both nanosecond[10] and picosecond lasers, then, the cross-section would have to be large. We hope to examine the fluence-dependent behavior of this feature using a shorter pulse (100 fs–1 ps) laser in the near future.

Photodissociation and dissociative photodetachment dynamics of O_6^-

The origin of the large change in the photodissociation dynamics between O_4^- and O_6^- at 532 nm constitutes an interesting question. As mentioned in the introduction, DeLuca *et al.*[9] interpreted the photodissociation of O_6^- in the absence of a significant absorption in O_4^- at 1064 nm in terms of a charge-transfer-to-solvent model. The current measurements by no means rule out such a mechanism at 1064 nm or any other wavelength. However, the observations in our laboratory of direct photodissociation of O_4^- on at least three repulsive ionic states[14] suggests that it is worthwhile to consider the change in dynamics in terms of a perturbation of the repulsive states of the molecular anion O_4^- by the addition of a third, weakly bound O_2. Additional evidence in favor of this interpretation comes from the marked similarity in the photodissociation dynamics of O_4^- and O_6^- at 355 nm. Photodissociation of both species yields high O_2^- vibrational excitation at 355 nm.

In the introduction the possible role played by the vibronically allowed ^2A_u repulsive state in the photodissociation of O_4^- and the production of highly vibrationally excited O_2^- at 355 nm was discussed. Given the similarity of the photodissociation dynamics of O_6^- at 532 and 355 nm to the 355 nm photodissociation dynamics of O_4^-, it is logical to consider a common origin for this behavior. The third O_2 might stabilize this repulsive state in the cluster relative to the $O_4^- \cdot O_2$ ground state. This stabilization could allow photoexcitation of this state at 532 nm in O_6^-, leading to the production of $O_2(^1\Delta_g) + O_2^-(^2\Pi_g, v)$. The energetics of this process in O_6^- must be carefully considered, however. Photodissociation of O_4^- at 532 nm produces $O_2(^1\Delta_g) + O_2^-(^2\Pi_g)$ with a maximum excess energy of 0.89 eV, of which 0.8 eV appears in translation. Thus, for O_4^-, the highest vibrational state of O_2^- energetically allowed is $v = 7$ (0.89 eV

above the zero point). However, Hiraoka has determined the binding energy of O_2 to O_4^- to be *ca.* 0.11 eV.[7] This result is consistent with the photoelectron spectra, and is likely to be chiefly due to stabilization of the ground state relative to the photo-dissociation asymptote. This shift is sufficient to rule out the production of $O_2^-(v = 7)$ from the photodissociation of $O_6^- \rightarrow O_2(^3\Sigma_g^-) + O_2(^1\Delta_g) + O_2^-(^2\Pi_g)$ at 532 nm.

A second explanation for the photodissociation dynamics of O_6^- at 532 nm is that the clustering of O_2 onto O_4^- opens up the energetically most stable photodissociation channel, producing $2O_2(^3\Sigma_g^-) + O_2^-(^2\Pi_g)$ at 532 nm. Given that this product channel must be operative to explain the photodissociation results reported by DeLuca *et al.*[9] at 1064 nm in O_6^-, this is plausible. As shown in Fig. 2, two dipole-allowed repulsive states in O_4^- correlate to this asymptote. Excitation to the $^2B_{3g}$ state will occur *via* a parallel transition, while the $^2B_{2g}$ state is reached by a perpendicular transition. In future measurements, we hope to determine the photofragment anisotropy for photodissociation of O_6^-, which should provide further insights into the possible role played by these lower-lying repulsive states in both O_4^- and O_6^-.

The increase in the photodissociation branching ratio relative to DPD as the third O_2 is added to O_4^- may be evidence for charge-transfer-to-solvent processes similar to those invoked by DeLuca *et al.*[9] in their studies below the photodetachment threshold for O_6^- at 1064 nm. The additional O_2 could serve to 'cage' the photodetached electron by capture to form vibrationally excited O_2^-, as shown by the electron attachment studies of neutral O_2 clusters by Märk and co-workers.[11] The electron attachment studies have shown that this process is only efficient for $E_{k, e} < 0.4$ eV, so it is possible that this process may consume the low energy electrons produced in the DPD of O_6^-. A second aspect of caging in the photodissociation of oxygen clusters is also worth consideration. A hard collision between the nascent O_2^- produced in photodissociation of the O_4^- core with the third O_2 might be expected to lead to vibrational excitation. The transfer of several quanta in such a collision is unlikely, however.[33] Furthermore, the near-two-body dynamics observed in the DPD of O_6^- at 266 nm indicate that collisional interactions with the third O_2 are likely to be negligible. In the future, we will carry out measurements of the vector correlations between the photofragments and photoelectrons produced in the photodestruction of O_6^-. If there are significant interactions with the third O_2 after photon absorption, by either a photodetached electron or the nascent O_2^-, little or no angular correlation will be observed between the products.

In contrast to the effect on the photodissociation dynamics, the dynamics of DPD appear to be only slightly perturbed by the addition of an O_2 to O_4^- at 266 nm. As the TOF measurements presented above show, DPD of O_6^- is a pseudo-two-body process, with minimal momentum transfer to the third O_2. While no calculations have been carried out on the structure of O_6^- to date, this observation alone can provide limited structural insights. At 266 nm, it is known that DPD in O_4^- occurs *via* a parallel transition, with the photofragments strongly peaked along the electric vector. The preservation of this behavior in O_6^- argues that the third O_2 must lie out of the plane of the O_4^- core, so the rapidly recoiling O_2 molecules produced in DPD of the core have only a minimal nearly elastic interaction with the third O_2.

5   Conclusions

Although the addition of a third O_2 to the O_4^- molecular anion has only a small effect on the ion stability, it is found to have a dramatic effect on the dynamics of ionic photodissociation. This is in marked contrast to the small effect observed on the dynamics of DPD. Further work, both experimental and theoretical, is required to fully describe the photodestruction processes at work in the anionic clusters of oxygen. While calculations of the electronic structure of these systems are difficult, reliable calculations for O_4^- have finally become available. Even in the case of O_4^- there have been no

theoretical studies of the dynamics of DPD and ionic photodissociation. An important test of the electronic structure and future dynamical studies of oxygen anions will be to explain in detail the dramatic effects on the photodissociation dynamics induced by the addition of an oxygen molecule to O_4^-.

Experimentally, further studies are in order to clarify the nature of three-body dissociation in O_6^-. This system is small enough to permit a detailed examination of the dynamics by a coincidence measurement of the energy and angular distributions of all the photofragments ($O_2 + O_2 + O_2 + e^-$). We have built an apparatus which will allow such measurements on this and other three-body cluster and molecular dissociation processes to be carried out. Such measurements should reveal the detailed nature of the partitioning of momentum among the three O_2 products, and should also provide the information required to distinguish between the charge-transfer-to-solvent mechanism proposed by DeLuca et al.,[9] and any role played by direct dissociation on the perturbed repulsive states of the molecular anion O_4^- 'solvated' by O_2. If the charge-transfer-to-solvent model is correct, it is doubtful that a large anisotropy in the $O_2 + O_2 + O_2^-$ product angular distributions will be observed. By carrying out these detailed measurements we plan on contributing to the growing understanding of the transition between gaseous and condensed phase systems. In addition, we hope that by providing a more detailed understanding of the chemistry of oxygen clusters, specific new insights into the chemistry of solid and liquid O_2 can be gained.

References

1 J. M. Farrar, in *Cluster Ions*, ed. T. Baer, C. Y. Ng and I. Powis, Wiley, New York, 1993, pp. 243–317.

2 A. W. Castleman, Jr. and K. H. Bowen, Jr., *J. Phys. Chem.*, 1996, **100**, 12911.

3 J. T. Snodgrass, C. M. Roehl and M. T. Bowers, *Chem. Phys. Lett.*, 1989, **159**, 10; T. Nagata and T. Kondow, *J. Chem. Phys.*, 1993, **98**, 290.

4 A. B. Jones, A. L. M. Buxey, P. R. Jukes, J. A. Smith and A. J. Stace, *J. Chem. Phys.*, 1995, **103**, 474.

5 V. Vorsa, S. Nandi, P. J. Campagnola, M. Larsson and W. C. Lineberger, *J. Chem. Phys.*, 1997, **106**, 1402.

6 B. J. Greenblatt, M. T. Zanni and D. M. Neumark, *Science*, 1997, **276**, 1675.

7 K. Hiraoka, *J. Phys. Chem.*, 1988, **89**, 3190.

8 L. A. Posey, M. J. DeLuca and M. A. Johnson, *Chem. Phys. Lett.*, 1986, **131**, 170.

9 M. J. DeLuca, C. C. Han and M. A. Johnson, *J. Chem. Phys.*, 1990, **93**, 268.

10 C. C. Han and M. A. Johnson, *Chem. Phys. Lett.*, 1992, **189**, 460.

11 S. Matejcik, A. Kiendler, P. Stampfli, A. Stamatovic and T. D. Märk, *Phys. Rev. Lett.*, 1996, **77**, 3771.

12 T. D. Märk, K. Leiter, W. Ritter and A. Stamatovic, *Phys. Rev. Lett.*, 1985, **55**, 2559.

13 K. A. Hanold, C. R. Sherwood and R. E. Continetti, *J. Chem. Phys.*, 1995, **103**, 9876.

14 C. R. Sherwood, K. A. Hanold, M. C. Garner, K. M. Strong and R. E. Continetti, *J. Chem. Phys.*, 1996, **105**, 10803.

15 K. A. Hanold, M. C. Garner and R. E. Continetti, *Phys. Rev. Lett.*, 1996, **77**, 3335.

16 R. N. Zare, *Mol. Photochem.*, 1972, **4**, 1.

17 K. A. Hanold, M. C. Garner and R. E. Continetti, unpublished work.

18 A. Aquino, S. P. Walch and P. R. Taylor, personal communication.

19 K. Andersson and B. O. Roos, in *Modern Electronic Structure Theory, Part 1*, ed. D. Yarkony, World Scientific Publishing, Singapore, 1995.

20 R. A. Kendall, T. H. Dunning and R. J. Harrison, *J. Chem. Phys.*, 1992, **96**, 6796.

21 K. A. Hanold, C. R. Sherwood, M. C. Garner and R. E. Continetti, *Rev. Sci. Instrum.*, 1995, **66**, 5507.

22 M. J. Travers, D. C. Cowles and G. B. Ellison, *Chem. Phys. Lett.*, 1989, **164**, 449.

23 K. P. Huber and G. Herzberg, *Molecular Spectra and Molecular Structure IV. Constants of Diatomic Molecules*, Van Nostrand, New York, 1979, pp. 506–507.

24 M. Allan, K. R. Asmis, D. B. Popovic, M. Stepanovic, N. J. Mason and J. A. Davies, *J. Phys. B: At. Mol. Opt. Phys.*, 1996, **29**, 3487.
25 G. J. Schulz, *Rev. Mod. Phys.*, 1973, **45**, 423.
26 M. Allan, *J. Phys. B: At. Mol. Opt. Phys.*, 1995, **28**, 5163.
27 U. Hefter, R. D. Mead, P. A. Schulz and W. C. Lineberger, *Phys. Rev. A*, 1983, **28**, 1429.
28 M. W. Siegel, R. J. Celotta, J. L. Hall, J. Levine and R. A. Bennett, *Phys. Rev. A*, 1972, **6**, 631.
29 K. J. Reed, A. H. Zimmerman, H. C. Andersen and J. I. Brauman, *J. Chem. Phys.*, 1976, **64**, 1368.
30 D. Dill, *J. Chem. Phys.*, 1976, **65**, 1130.
31 R. L. Jackson, P. C. Hiberty and J. I. Brauman, *J. Chem. Phys.*, 1981, **74**, 3705.
32 C. G. Bailey, C. E. H. Dessent, M. A. Johnson and K. H. Bowen, Jr., *J. Chem. Phys.*, 1996, **104**, 6976.
33 X. Yang, J. M. Price, J. A. Mack, C. G. Morgan, C. A. Rogaski, D. McGuire, E. H. Kim and A. M. Wodtke, *J. Phys. Chem.*, 1993, **97**, 3944.